Performance of Miniature Implantable Antennas for Medical Telemetry at 402, 433, 868 and 915 MHz

Asimina Kiourti and Konstantina S. Nikita

National Technical University of Athens, School of Electrical and Computer Engineering
akiourti@biosim.ntua.gr, knikita@ece.ntua.gr

Abstract. In this paper, we compare the performance of implantable antennas for integration into implantable medical devices and telemetry in the MICS (402.0–405.0 MHz) and ISM (433.1–434.8, 868.0–868.6 and 902.8–928.0 MHz) bands. A parametric model of a miniature (volume of 32.7 mm^3) patch antenna is proposed for skin–implantation, and further refined for each frequency set–up. Implantation inside canonical models of the human head, arm and trunk is considered, and the antenna resonance, radiation and safety performance is compared. Results indicate enhanced bandwidth and improved radiation and safety performance at higher frequencies because of the increased copper surface area. Implantation of a specific antenna inside different parts of the human body is shown to insignificantly affect its performance.

Keywords: arm, Finite Element (FE), head, implantable antenna, Implantable Medical Device (IMD), Industrial Scientific and Medical (ISM) band, Medical Implant Communications Service (MICS) band, medical telemetry, trunk.

1 Introduction

Medical telemetry permits the measurement of physiological signals at a distance, through either wire or wireless communication technologies. One of its latest applications is in the field of Implantable Medical Devices (IMDs), which are used to perform an expanding variety of diagnostic and therapeutic functions (e.g. pacemakers [1], Functional Electrical Stimulators (FES) [2], blood glucose sensors [3] etc). In the past, wireless medical telemetry for IMDs relied on inductive coil coupling [4]. To overcome the inherent drawbacks of low data rate (1–30 kb/s), restricted communication range (less than 10 cm), and sensitivity to coils' positioning, research is currently oriented towards antenna–enabled medical telemetry for IMDs (e.g. [5]–[7]).

The ITU–R Recommendation SA.1346 [8] has outlined the use of the 402–405 MHz frequency band for Medical Implant Communications Systems (MICS). The MICS band attracts high scientific interest because of its advantages to be internationally available and feasible with low power circuits, reliably support high data rate transmissions, fall within a relatively low noise portion of the spectrum, and propagate acceptably through human tissue. The 433.1–434.8, 868.0–868.6 and 902.8–928.0 MHz Industrial Scientific and Medical (ISM) bands are also suggested for IMD telemetry in some countries [9].

B. Godara and K.S. Nikita (Eds.): MobiHealth 2012, LNICST 61, pp. 122–129, 2013.

In this study, we propose a parametric model of a miniature patch antenna for skin–implantation [10], and tune its parameters inside a canonical head model to obtain antennas at 402, 433, 868 and 915 MHz. Implantation inside canonical models of the human arm and trunk is also considered, and antenna performance is compared in terms of resonance (bandwidth), radiation (far–field radiation pattern and exhibited gain) and safety (conformance with the IEEE C95.1–1999 and C95.1–2005 [11] safety guidelines). Numerical simulations are carried out using the Finite Element (FE) method.

The paper is organized as follows. Section 2 describes the models and numerical method used in this study. Numerical results are presented and discussed in Section 3. The paper concludes in Section 4.

2 Models and Numerical Method

2.1 Antenna and Tissue Models

The parametric antenna model of Fig. 1 is proposed for designing the 402, 433, 868 and 915 MHz implantable antennas of this study. The model is a modified version of the one presented by the authors in [7], emphasizing on miniaturization and biocompatibility. Miniaturization techniques including patch stacking, meandering and addition of a shorting pin are applied to reduce the antenna volume to 32.7 mm^3. Biocompatible alumina (dielectric constant, $\varepsilon_r = 9.4$, and loss tangent, $\tan\delta = 0.006$), which has long been used in implantable antenna design [12], [13], is chosen as the dielectric material. Throughout this paper, the origin of the coordinate system is located at the center of the antenna ground plane, as shown in Fig. 1.

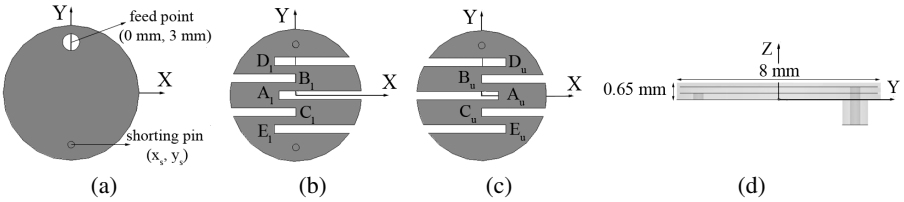

Fig. 1. Proposed parametric antenna model: (a) ground plane, (b) lower patch, (c) upper patch, and (d) side view

The antenna model consists of a 4 mm–radius ground plane and two 3.9 mm–radius vertically–stacked meandered patches, which are both fed by a 50–Ohm coaxial cable (x = 0 mm, y = 3 mm). Patches are printed on 0.25 mm–thick substrates, while a 0.15 mm–thick superstrate covers the structure to preserve its biocompatibility and robustness. Meanders are equi–distant by 1 mm, their width is fixed to 0.5 mm, and their lengths are considered variable (denoted by the x coordinate (x_{ij}), where the subscripts {ij, i = A–F, j = L, U} identify the meander in Fig. 1(b) and (c)). A variably–positioned shorting pin ($x = x_s$, $y = y_s$) connects the ground plane with the lower patch. Tuning the x_{ij}, x_s and y_s variables alters the effective dimension of the antenna and helps achieve the desired resonance characteristics.

Antenna performance is evaluated inside the skin–tissue of canonical head, arm, and trunk models for applications such as intra–cranial pressure, blood pressure, and glucose monitoring, respectively. The following tissue models are considered:

(a) a spherical head model consisting of skin (thickness of 5 mm), bone (thickness of 5 mm), and grey matter tissues (Fig. 2(a) [7],

(b) a cylindrical arm model consisting of skin (thickness of 5 mm), muscle (thickness of 25 mm), and bone tissues (Fig. 2(b)) [14], and

(c) an ellipsoidal trunk model consisting of skin (thickness of 5 mm), fat (thickness of 10 mm), and muscle tissues (Fig. 2(c)) [15].

Tissue electric properties at f_0 (f_0 = 402, 433, 858, 915 MHz) are considered (Table 1 [16]), and approximated as constant inside a ±100 MHz frequency range around f_0 [7]. Tissue mass densities are also provided in Table 1. Effect of the tissue anatomy and dielectric parameters is expected to be of minor importance, as indicated by the authors in [17].

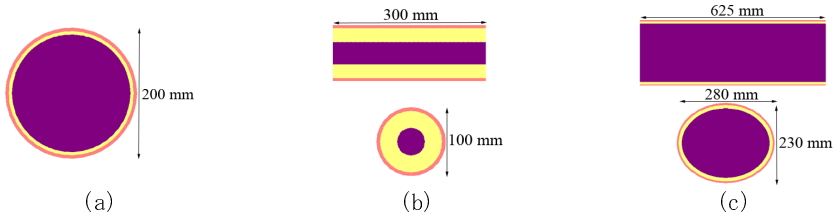

Fig. 2. Canonical models of the human: (a) head [7], (b) arm [14], and (c) trunk [15]

Table 1. Electric properties (permittivity, ε_r, and conductivity, σ) [16] and mass density of the tissues used in this study

Tissue type	402 MHz		433 MHz		868 MHz		915 MHz		Mass Density
	ε_r	σ [S/m]	ε_r	σ [S/m]	ε_r	σ [S/m]	ε_r	σ [S/m]	[kg/m^3]
skin	46.74	0.689	46.08	0.702	41.58	0.856	41.33	0.872	1100
bone	13.10	0.090	13.07	0.094	12.48	0.139	12.44	0.145	2200
grey matter	57.39	0.738	56.83	0.751	52.88	0.929	52.65	0.949	1030
muscle	57.11	0.797	56.87	0.805	55.11	0.932	54.99	0.948	1040
fat	5.58	0.041	5.57	0.042	5.47	0.050	5.46	0.051	920

2.2 Numerical Method

Simulations are carried out using the Finite Element method [18], which has been extensively used in the literature to study the design and performance of implantable antennas (e.g. [5], [7]). The mesh is automatically refined by the FE solver in an iterative way. A maximum perturbation of 30% is performed between each iteration, and the mesh refinement procedure stops when the maximum change in the magnitude of the reflection coefficient ($|S_{11}|$) between two consecutive iterations is less than 0.02, or when the number of iterations exceeds 10. Radiation boundaries are set $\lambda_0/4$ (λ_0 is the free–space wavelength, f_0 = 402 MHz) away from all simulation

set–ups in order to extend radiation infinitely far and guarantee stability of the numerical calculations.

3 Numerical Results

3.1 Antenna Design and Resonance Performance

The parametric antenna model of Fig. 1 is implanted by 2.5 mm under the skin–tissue of the canonical head model (Fig. 2(a)), and its parameter (x_{ij}, x_s, and y_s) values are manually updated in an iterative way, until the magnitude of the reflection coefficient ($|S_{11}|$) at the desired resonance frequency (f_0) is adequately low, as dictated by:

$$\left|S_{11}\right|_{@\, f_0} \leq -20 \text{ dB} \tag{1}$$

In this way, four antennas are obtained for scalp–implantation and medical telemetry at 402, 433, 868, and 915 MHz, respectively, as shown in Fig. 3 and Table 2. Longer meanders increase the length of the current flow path on the antenna, decreasing, in turn, the exhibited resonance frequency. The patch surface area of the 433, 868 and 915 MHz antennas is found to be increased by 2.2%, 24.9% and 25.4% as compared to that of the 402 MHz antenna.

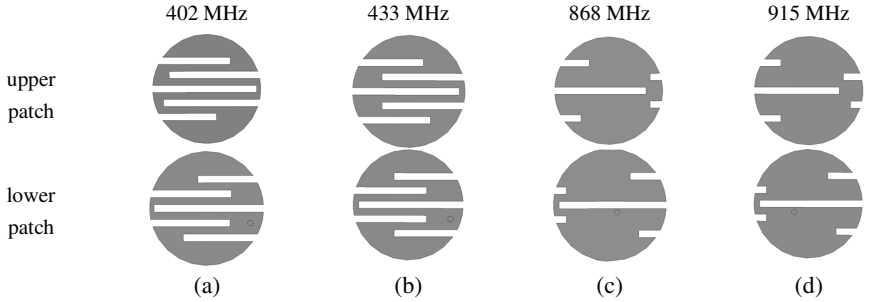

Fig. 3. Geometries of the proposed antennas at: (a) 402, (b) 433, (c) 868, and (d) 915 MHz

The reflection coefficient frequency responses of the proposed antennas inside the head model (Fig. 2(a)) are shown in Fig. 4(a). Further implantation of these designs by 2.5 mm under the skin–tissue of the arm (Fig. 2(b)) and trunk (Fig. 2(c)) models causes insignificant changes in the exhibited resonance performance, as shown in Fig. 4(b) and Fig. 4(c). The computed values for the 10 dB–bandwidth (i.e. the bandwidth defined at a return loss of 10 dB) of the antennas are indicated in Table 3 for all frequency set–ups and implantation scenarios of this study. Original values are recorded, while percent changes from the values of the 402 MHz antenna are given in parentheses. Bandwidth improvement with increasing frequency is attributed to the larger current surface area of the patches, as shown in Fig. 3.

Table 2. Variable values of the proposed antenna designs

Var.	Values [mm]			
	402 MHz	*433 MHz*	*868 MHz*	*915 MHz*
x_{Al}	–3.6	–3.5	–3.5	–3.4
x_{Bl}	1.7	1.3	–3	–3
x_{Cl}	1.6	1.3	–3	–3
x_{Dl}	–0.6	–1	1.4	1.4
x_{El}	–1.6	–1	2	2
x_{Au}	3.6	3.5	2.6	2.2
x_{Bu}	–2.7	–1.9	3	2.5
x_{Cu}	–3.1	–1.9	3	3
x_{Du}	1.7	1	–1.4	–2
x_{Eu}	0.7	1.5	–2	–2
(x_s, y_s)	(3, –1)	(3, –1)	(0.5, –0.5)	(–1, –0.6)

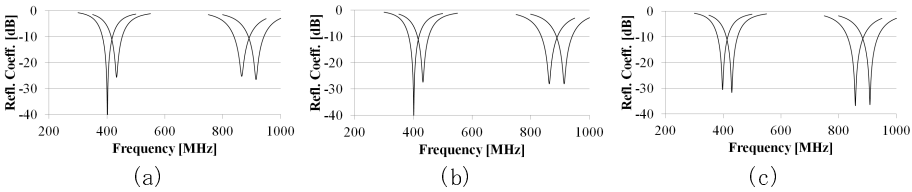

Fig. 4. Reflection coefficient frequency responses of the proposed antennas inside the human: (a) head (Fig. 2(a)), (b) arm (Fig. 2(b)), and (c) trunk (Fig. 2(c))

Table 3. 10 dB–Bandwidth (in [MHz]) of the proposed antennas for all frequency set–ups and implantation scenarios of this study

Implantatio Scenario	Frequency Set–Up			
	402 MHz	*433 MHz*	*868 MHz*	*915 MHz*
Head	35.2	38.4 (+9.1%)	53.3 (+51.4%)	54.3 (+54.3%)
Arm	35.3	38.7 (+9.6%)	53.7 (+52.1%)	55.1 (+56.1%)
Trunk	35.4	39.3 (+11.0%)	54.7 (+54.5%)	56.1 (+58.5%)

3.2 Radiation Performance

The three–dimensional far–field gain radiation patterns of the proposed antennas are shown in Fig. 5 for all frequency set–ups and implantation scenarios of this study. A near–zone to far–field transformation is used to speed–up calculations. Since the antennas are electrically very small, they radiate nearly omni–directional, monopole–like radiation patterns. The maximum exhibited far–field gain values are given in Table 4. Original values are recorded, while percent changes from the values of the 402 MHz antenna are given in parentheses. Low gain values are computed because of the miniaturized antenna dimensions. Higher gain values with increasing frequency are attributed to the larger current surface area of the patches, as indicated in Fig. 3.

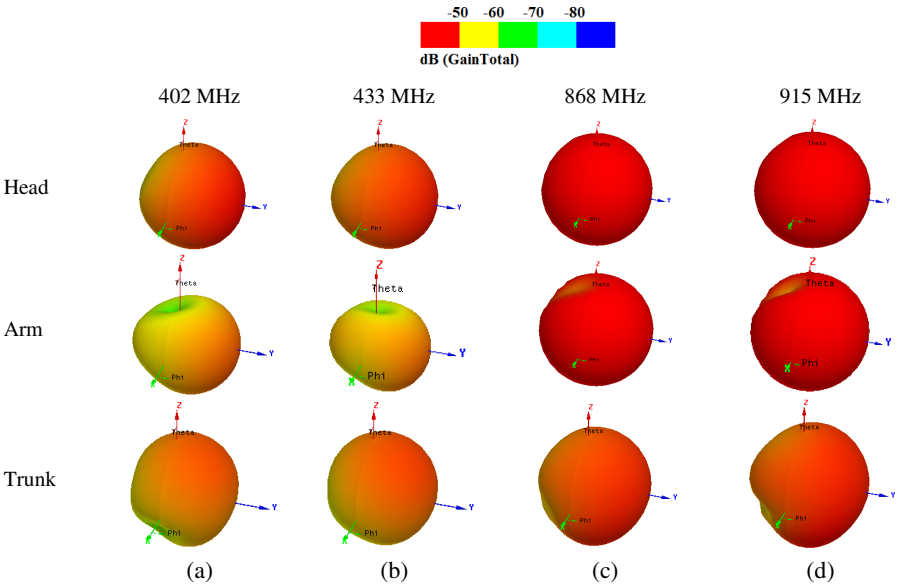

Fig. 5. Far–field gain radiation patterns of the proposed antennas for all implantation scenarios, at: (a) 402, (b) 433, (c) 868, and (d) 915 MHz

Table 4. Maximum far–field gain values (in [dB]) exhibited by the proposed antennas for all frequency set–ups and implantation scenarios of this study

Implantatio Scenario	Frequency Set–Up			
	402 MHz	**433 MHz**	**868 MHz**	**915 MHz**
Head	–50.98	–50.25 (+1.4%)	–41.90 (+17.8%)	–41.36 (+18.9%)
Arm	–54.16	–53.74 (+0.8%)	–42.56 (+21.4%)	–41.96 (+22.5%)
Trunk	–53.26	–52.69 (+1.1%)	–41.35 (+27.5%)	–40.07 (+28.4%)

3.3 Safety Performance

Issues related to patient safety limit the maximum allowable power incident to an implantable antenna. The Specific Absorption Rate (SAR) (rate of energy deposited per unit mass of tissue) is generally accepted as the most appropriate dosimetric measure, and compliance with international guidelines is assessed. For example, the IEEE C95.1–1999 standard restricts the SAR averaged over any 1 g of tissue in the shape of a cube to less than 1.6 W/kg, while the IEEE C95.1–2005 standard restricts the SAR averaged over any 10 g of tissue in the shape of a cube to less than 2 W/kg [11].

In order to determine the maximum allowable net–input power levels to the proposed implantable antennas, an SAR numerical analysis is carried out for all frequency set–ups and implantation scenarios of this study. The net–input power is initially set to 1 W and the maximum 1 g– and 10 g–averaged SAR values are

computed, based on numerical computational procedures recommended by IEEE [19]. In order to guarantee conformance with the IEEE C95.1–1999 and the IEEE C95.1–2005 standards [11], the power incident to the antenna should be decreased to the levels indicated as P_{1999} and P_{2005} in Table 5, respectively. Original values are recorded, while percent changes from the values of the 402 MHz antenna are given in parentheses. The old IEEE C95.1–1999 standard is found to be much stricter, limiting the net–input power to more than 10 times lower than that imposed by the recent IEEE C95.1–2005 standard. At higher operation frequencies, electric field, or, equivalently, current density, is more uniformly distributed across an increased surface area of the radiating patches, as indicated in Fig. 3. Lower maximum SAR values, or equivalently, higher maximum allowable net–input power levels are, thus, computed.

Table 5. Maximum allowable net–input power to the proposed antennas which guarantees conformance with the IEEE C95.1–1999 (P_{1999}) and C95.1–2005 (P_{2005}) [11] standards (in [mW]), for all frequency set–ups and implantation scenarios of this study

Implantation Scenario	Frequency Set–Up							
	402 MHz		***433 MHz***		***868 MHz***		***915 MHz***	
	P_{1999}	P_{2005}	P_{1999}	P_{2005}	P_{1999}	P_{2005}	P_{1999}	P_{2005}
Head	1.664	20.853	1.672 (+0.48%)	20.927 (+0.35%)	1.685 (+1.26%)	21.338 (+2.33%)	1.714 (+3.00%)	21.409 (+2.67%)
Arm	1.676	20.951	1.680 (+0.24%)	21.008 (+0.27%)	1.724 (+2.86%)	21.470 (+2.48%)	1.727 (+3.04%)	21.531 (+2.77%)
Trunk	1.678	20.962	1.686 (+0.48%)	21.033 (+0.34%)	1.726 (+2.86%)	21.559 (+2.85%)	1.729 (+3.04%)	21.529 (+2.71%)

4 Conclusion

A parametric model of a skin–implantable antenna was proposed, emphasizing on size miniaturization and biocompatibility, and further refined for implantation inside the skin–tissue of a canonical head model and medical telemetry at 402, 433, 868 and 915 MHz. Implantation of the same antenna inside different implantation scenarios (head, arm, trunk) was shown to cause minor changes to the exhibited resonance, radiation and safety performance. On the other hand, the operation frequency of the antenna was found to be relatively significant: antennas at higher frequencies were shown to exhibit enhanced bandwidths, higher gains, and increased maximum allowable input power levels imposed by international safety guidelines. Results are attributed to the enhanced patch surface area of the antennas at higher frequencies.

References

1. Wessels, D.: Implantable pacemakers and defibrillators: Device overview and EMI considerations. In: IEEE Int. Symp. Electromagn. Compat. Conference (2002)

2. Guillory, K., Normann, R.A.: A 100–channel system for real time detection and storage of extracellular spike waveforms. J. Neurosci. Methods 91, 21–29 (1999)
3. Shults, M.C., Rhodes, R.K., Updike, S.J., Gilligan, B.J., Reining, W.N.: A telemetry–instrumentation system for monitoring multiple subcutaneously implanted glucose sensors. IEEE Trans. Biomed. Eng. 41, 937–942 (1994)
4. Tang, Z., Smith, B., Schild, J.H., Peckham, P.H.: Data transmission from an implantable biotelemeter by Load-Shift Keying using circuit configuration modulator. IEEE Trans. Biomed. Eng. 42, 524–528 (1995)
5. Karacolak, T., Hood, A.Z., Topsakal, E.: Design of a dual–band implantable antenna and development of skin mimicking gels for continuous glucose monitoring. IEEE Trans. Microw. Theory Techn. 56, 1001–1008 (2008)
6. Sánchez–Fernández, C.J., Quavado–Teruel, O., Requena–Carrión, J., Inclán–Sánchez, L., Rajo–Iglesias, E.: Dual–band microstrip patch antenna based on short 0 circuited ring and spiral resonators for implantable medical devices. IET Mikrow. Antennas Propag. 4, 1048–1055 (2010)
7. Kiourti, A., Nikita, K.S.: Miniature Scalp–Implantable Antennas for Telemetry in the MICS and ISM Bands: Design, Safety Considerations and Link Budget Analysis. IEEE Trans. Antennas Propag. 60, 3568–3575 (2012)
8. International Telecommunications Union-Radiocommunications, radio regulations, SA.1346, ITU, Geneva, Switzerland, http://itu.int/home
9. International Telecommunications Union-Radiocommunications, radio regulations, section 5.138 and 5.150, ITU, Geneva, Switzerland, http://itu.int/home
10. Kiourti, A., Nikita, K.S.: A Review of Implantable Patch Antennas for Biomedical Telemetry: Challenges and Solutions. IEEE Antennas Propag. Mag. 54, 210–228 (2012)
11. IEEE Standard for Safety Levels with Respect to Human Exposure to Radiofrequency Electromagnetic Fields, 3kHz to 300 GHz, IEEE Standard C95.1 (1999) (2005)
12. Capello, W.W., D'Anthonio, J., Feinberg, J., Manley, M.: Alternative Bearing Surfaces: Alumina Ceramic Bearings for Total Hip Arthroplasty. In: Benazzo, F., Falez, F., Dietrich, M. (eds.) Bioceramics and Alternative Bearings in Joint Arthroplasty, pp. 87–94. Springer (2005)
13. Kiourti, A., Christopoulou, M., Nikita, K.S.: Performance of a novel miniature antenna implanted in the human head for wireless biotelemetry. In: IEEE Int. Symp. Antennas Propag. (2011)
14. Wegmueller, M.S., Oberle, M., Kuster, N., Fichtner, W.: From dielectrical properties of human tissue to intra–body communications. In: World Congress Med. Physics Biomed. Eng. (2006)
15. Shiba, K., Nukaya, M., Tsuji, T., Koshiji, K.: Analysis of current density and specific absorption rate in biological tissue surrounding transcutaneous transformer for an artificial heart. IEEE Trans. Biomed. Eng. 55, 205–213 (2008)
16. Gabriel, C., Gabriel, S., Corthout, E.: The dielectric properties of biological tissues. Phys. Med. Biol. 41, 2231–2293 (1996)
17. Kiourti, A., Nikita, K.S.: Numerical Assessment of the Performance of a Scalp-Implantable Antenna: Effects of Head Anatomy and Dielectric Parameters. Wiley Bioelectromagnetics (to appear), doi:10.1002/bem.21753
18. Sadiku, M.N.O.: Numerical techniques in electromagnetic. CRC Press (2001)
19. IEEE Recommended Practice for Measurements and Computations of Radio Frequency Electromagnetic Fields with Respect to Human Exposure to such Fields, 100 kHz to 300 GHz, IEEE Standard C95.3–2002 (2002)